Robust Design Optimization of Switched Reluctance Motor Drive Systems Based on System-Level Sequential Taguchi Method

Kaikai Diao, *Student Member, IEEE*, Xiaodong Sun, *Senior Member, IEEE*, Gang Lei, *Member, IEEE*, Gerd Bramerdorfer, *Senior Member, IEEE*, Youguang Guo, *Senior Member, IEEE*, and Jianguo Zhu, *Senior Member, IEEE*

***Abstract*—In this paper, a new system-level sequential Taguchi method (SLSTM) is proposed to achieve the optimal solution with high robustness for switched reluctance motor (SRM) drive systems. An SRM drive system consisting of a segmented-rotor SRM and the angle position controller is investigated as a case study. In the implementation, the optimization function contains torque, loss, and torque ripple. The control factors of the system are selected according to the sensitivity analysis results. Manufacturing tolerances are considered to guarantee that the optimal solution features low sensitiveness to uncertainties. The process of defining the design levels of all the control factors and noise factor is illustrated and the orthogonal array is established. The optimization of the SLSTM is carried out sequentially until the certain convergence condition is satisfied. Finally, the component-level sequential Taguchi method (CLSTM) is carried out for comparison. It appears that the proposed SLSTM is efficient in searching for the robust optimal solution for the SRM drive system. Besides, it can achieve better output performance, such as higher average torque and lower torque ripple, and a higher level of robustness compared with the initial design and CLSTM.**

***Index Terms*—Manufacturing tolerances, robust design, switched reluctance motor (SRM), Taguchi method.**

I. Introduction

ELECTRIC vehicles (EVs) and hybrid EVs (HEVs) are achieving increasing attention and market share with the development and application of high-reliability motors [1], [2]. During recent years, switched reluctance motors (SRMs) have aroused increased interests thanks to the benefits of rigid structure, high robustness, the absence of permanent magnets, and low manufacturing cost. SRMs provide an alternative to traditional electric machines like permanent magnet motors and inductance motors in EVs and HEVs [3], [4]. Conventional SRMs with doubly salient structure have been designed and tested on EVs or HEVs [5], [6]. Besides, a variety of novel topologies have been derived from the conventional structure, including the SRMs with segmented stator/rotor [7], [8] and double stator [9].

To provide excellent drive performance to meet the challenging requirements, SRMs should be properly designed and optimized before application. Previous research efforts on the design and optimization of SRMs mainly focus on a single performance index, such as torque ripple [10], loss [11] or efficiency [12]. However, focusing on a single objective typically has significant adverse effects on other important performance measures [13], [14]. Consequently, the multiobjective optimization method has been widely applied, which allows simultaneously considering different optimization targets at once. Thus, their respective trade-off can be analyzed, and it facilitates to accommodate the needs for different applications [15], [16].

To find the overall best solution and tackle the high-dimensional problem in a computationally efficient manner, intelligent algorithms, such as genetic algorithm (GA) [17] and particle swarm optimization (PSO) [18], are favourable in the case of multiobjective optimization problems. Commonly, intelligent algorithms are coupled with a finite element solver to allow an accurate solving of respective multiobjective optimization problems. Furthermore, several surrogate modeling techniques, such as response surface (RS) [19] and Kriging based approaches [20], [21], can be applied to reduce the computational burden. For example, a comprehensive framework for multiobjective design optimization of SRMs based on a combination of the RS model and PSO approach has been proposed in [22]. A sample SRM with multiple objectives, i.e., the maximization of the torque per active mass and

Manuscript received October 01, 2020; revised March 17, 2021; accepted May 27, 2021. This work was supported in part by the National Natural Science Foundation of China under Project 51875261, in part by the Natural Science Foundation of Jiangsu Province of China under Project BK20180046, in part by the Postgraduate Research & Practice Innovation Program of Jiangsu Province under Project KYCX20_3014, and in part by the State Scholarship Fund of China Scholarship Council under Grant 202008320572. (*Corresponding author: Xiaodong Sun*.)

K. Diao and X. Sun are with the Automotive Engineering Research Institute, Jiangsu University, Zhenjiang 212013, China (email: diaokaikai@163.com, xdsun@ujs.edu.cn).

G. Lei and Y. Guo are with the School of Electrical and Data Engineering, University of Technology Sydney, NSW 2007, Australia (e-mail: Gang.Lei@uts.edu.au, Youguang.Guo-1@uts.edu.au).

Gerd Bramerdorfer is with the Department of Electrical Drives and Power Electronics, Johannes Kepler University Linz, Linz 4040, Austria (email: gerd.bramerdorfer@jku.at).

J. Zhu is with the School of Electrical and Information Engineering, University of Sydney, NSW, 2006, Australia (e-mail: jianguo.zhu@sydney.edu.au).

efficiency, while simultaneously minimizing torque ripple, is optimized to show the reliability of the proposed method.

Due to manufacturing tolerances and material diversity, variations of the design variables are unavoidable when producing SRMs. Mass production of SRMs with higher quality is a key requirement for decreasing the possibility of failure [23]. Six-sigma robust optimization method is an effective way to deal with optimization problems featuring unavoidable uncertainties in industrial manufacturing. In [24], a robust design optimization approach was presented by incorporating the methodology of design for six sigma, and it is verified by an example of a transverse flux machine. The reliability and quality levels of an investigated example can be significantly improved. However, it requires abundant finite element analysis based evaluations, which leads to high computational cost. Compared with the six-sigma robust optimization method, the Taguchi design approach based on orthogonal array exhibits high computational efficiency since it does not use complicated algorithms and additional programming. Taguchi approach has been successfully employed to optimize different kinds of motors, such as interior permanent magnet synchronous motors [25], [26], and SRMs [27].

The main drawback of the conventional Taguchi method is that the selection of the values and the improvement of performance significantly depend on the defined levels which highly dependent on the number of levels and human experience. Moreover, previous work on the Taguchi method only considered the parameters for the motor domain but ignored the parameters of the controller, which can be regarded as a component-level Taguchi method rather than a system-level Taguchi method.

To solve the drawback of the conventional Taguchi method and achieve the robust optimal solution for the whole drive system, in this paper, an efficient robust design optimization method is presented for SRM drive systems. A design example with a segmented-rotor SRM (SSRM) will be investigated to present the effectiveness of the SLSTM. The main contribution of this paper is that a novel system-level sequential Taguchi method (SLSTM) is proposed to achieve a robust design for the whole SRM drive system including the parameters in ontology and control aspects. The proposed method can improve the reliability and quality of products in batch production.

The remainder of this article is organized as follows. The design example is described in Section II. The SLSTM applied to the SSRM is investigated in Section III. Results and comparison between initial design, component-level sequential Taguchi method (CLSTM) and SLSTM are presented in Section IV. Finally, the main findings are summarized in the conclusion in Section V.

II. The Design Example

The SSRM was first proposed in [28]. It was demonstrated that the SSRM provides the potential for a great improvement in torque density compared with the SRM with a conventional toothed rotor structure. The static characteristics and operational test results have been presented to explain why the SSRM exhibits superior performance. Furthermore, in [29], a strategy was developed for the SSRM to maximize its efficiency. The optimization applies a combination of static and dynamic analysis to ensure a comprehensive optimization of the machine. In [30], a novel 6/5 SSRM was investigated for cooling fan application. The stator is divided into excited poles and auxiliary poles, which further improves efficiency. The principle of design and operation was investigated. A comparison shows that the SSRM can exhibit higher electrical utilization than the conventional SRM.

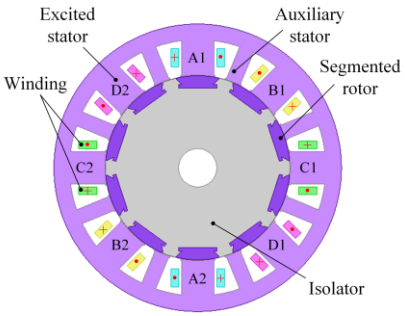

Fig. 1. The FEM of the SSRM.

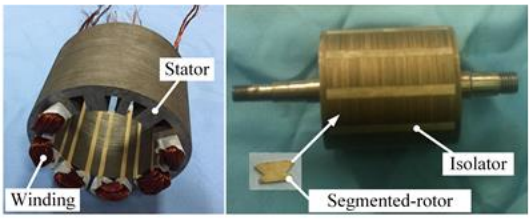

Fig. 2. The topology of the SSRM.

TABLE I
SPECIFICATIONS OF THE SSRM

Parameters	Unit	value
Rated power	kW	1.8
Rated speed	r/min	6000
Rated voltage	V	60
Efficiency at rated speed	-	0.85

TABLE II
INITIAL DESIGN OF THE SSRM

Par.	Description	Unit	Value
N_{ph}	Phase number	-	4
N_s	Stator poles number	-	16
N_r	Rotor poles number	-	10
D_{so}	Stator outer diameter	mm	128
l	Axial length	mm	80
D_{ro}	Rotor outer diameter	mm	82
β_{s1}	Excited stator pole arc	deg.	21.4
β_{s2}	Auxiliary stator pole arc	deg.	10.7
β_r	Rotor pole arc	deg.	26.6
L_{sy}	Stator yoke	mm	7
h_{cr}	Segmented rotor height	mm	5.5
g	Air gap	mm	0.25
n	Number of turns	-	24
θ_{on}	Turn-on angle	deg.	-3
θ_{off}	Turn-off angle	deg	12

In our previous work, a 16/10 stator/rotor poles SSRM was designed and investigated [7], [21]. Figs. 1 and 2 show the finite element model (FEM) and the topology of the SSRM, respectively. Compared with a conventional SRM with a doubly salient structure, the rotor of the SSRM is composed of a series of discrete segmented rotors which are embedded in a nonmagnetic isolator. Besides, the stator teeth of the SSRM can be categorized into two types. One is the excited stator tooth featuring a tooth-wound coil, and the other is the auxiliary pole without any coil. The function of the auxiliary poles is to provide the return flux path for the excited poles. The specifications and the initial design of the SSRM are tabulated in Tables I and II, respectively.

Theoretically, it is a big challenge to validate the robust optimal results experimentally as the production environment should be developed, instead of the laboratory prototype environment, for the mean and standard deviation information. An alternative way is to validate all FEM analysis models and uncertainty data related to manufacturing tolerances employed in the optimization. The optimal results should be reliable if all of these can be validated.

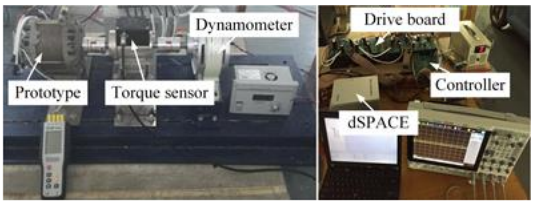

Fig. 3. Experimental platform.

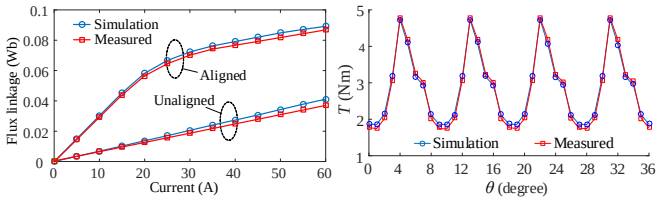

Fig. 4. Simulation and measured results. (a) Flux linkage. (b) Dynamic torque at rated condition under angle position control (APC).

Fig. 3 shows the experimental platform. The simulation and measured results of flux linkage and dynamic torque are shown in Fig. 4. The simulation and measured values are in good agreement. In this work, the simulation model is established in Ansoft/Maxwell. The simulated copper loss and core loss are 104 W and 127 W respectively, while the measured copper loss and core loss are about 109 W and 135 W respectively at the rated operation, and the coil temperature is about 59.8 °C. The errors of the copper loss and core loss between simulation and experiment are about 4.8% and 6.3%, respectively. All the experimental results have verified the effectiveness of this FEM-based analysis method. Thus, it is reliable to use FEM results to investigate the system-level optimization process.

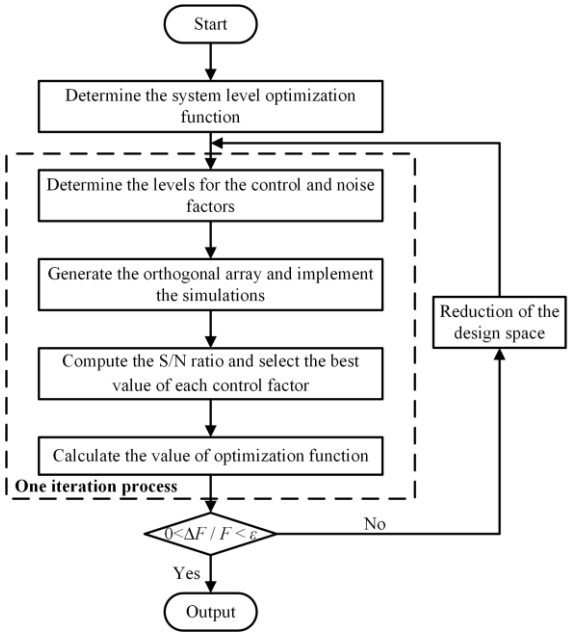

Fig. 5. The flowchart of the SLSTM.

III. System-Level Sequential Taguchi Method

Fig. 5 presented the optimization flowchart of the proposed system-level sequential Taguchi method (SLSTM). It can be divided into the following six steps.

Step 1: Determine the system-level optimization function.

For a design optimization problem, the optimization function should be determined first. In this example, three objectives, i.e., torque, loss, and torque ripple are selected as the optimization objectives since they are the main obstacles for the wide application of SRMs in the industry. These three objectives can be combined into one optimization function, which can be defined as

$$\begin{aligned} \min:\ & F(\mathbf{x}_s) = w_1 \frac{T_{avg\_initial}}{T_{avg}} + w_2 \frac{P_{loss}}{P_{loss\_initial}} + w_3 \frac{T_{ripple}}{T_{ripple\_initial}} \\ \text{s.t.}\ & g_1(\mathbf{x}_s) = sf - 0.6 \le 0 \\ & g_2(\mathbf{x}_s) = T_{\text{coil}} - 75 \le 0 \\ & \mathbf{x}_{sl} \le \mathbf{x}_s \le \mathbf{x}_{su} \end{aligned} \quad (1)$$

where $T_{avg\_initial}$, $P_{loss\_initial}$, and $T_{ripple\_initial}$ are the average torque, loss and torque ripple of the initial design, respectively, $\mathbf{x}_s$ is the vector space of the design variables, and g_i is the constraints, respectively, $\mathbf{x}_{sl}$ and $\mathbf{x}_{su}$ are the lower and upper boundaries, respectively, sf and T_{coil} (in °C) represent the slot fill factor and the temperature of the coil, respectively, and w_1, w_2, and w_3 are the weighting factors. In this example, the torque is set as the prime objective, followed by the loss and torque ripple, thus, w_1, w_2, and w_3 are assigned as 0.4, 0.3, and 0.3, respectively. The loss in (1) is the sum of the copper loss and core loss.

Fig. 6 presents a thermal network model for the investigated SSRM. R_h, R_{sy}, R_{st}, R_r, and R_g are the equivalent thermal resistances of the housing, the stator yoke, the stator tooth, the rotor and the airgap, respectively. The heat sources in this model include the stator yoke core loss (P_{sy}), the stator teeth core loss (P_{st}), the rotor core loss (P_r), and the copper loss (P_{cu}),

which can be achieved from FEM during the optimization process.

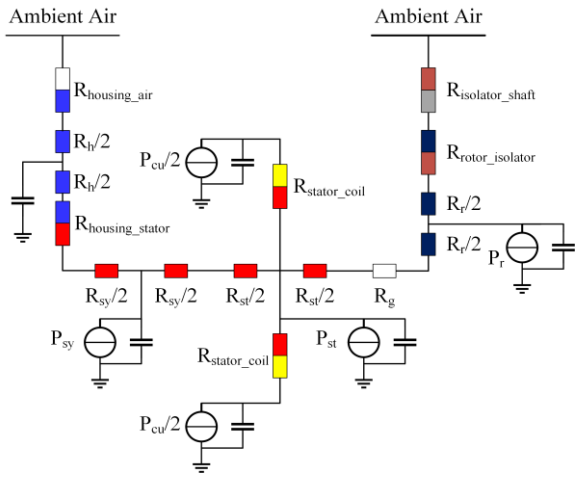

Fig. 6. Thermal network model of the SSRM.

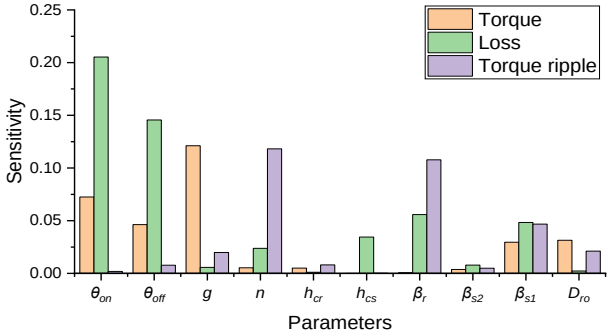

Fig. 7. Sensitivity indices.

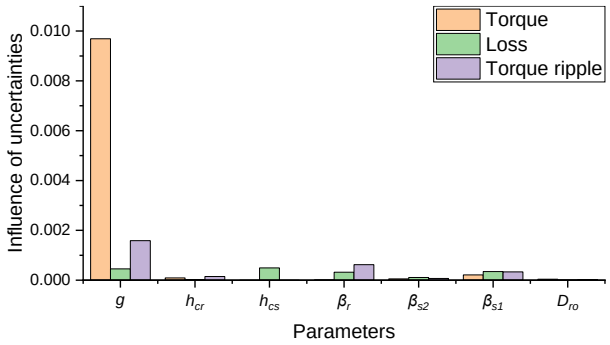

Fig. 8. Influence of uncertainties.

Step 2: Determine the levels for control and noise factors.

The control factors will be selected according to the sensitivity analysis of design parameters on each optimization objective. It should be noted that for the proposed SLSTM, the design parameters contain the parameters in motor level and control level, which jointly allow for a system-level optimization. The sensitivity of parameter x_i can be achieved by

$$S(x_i) = \frac{V(E(f/x_i))}{V(f)} \tag{2}$$

where f is the optimization objective, $E(f/x_i)$ is the average value of f when x_i is constant, $V(E(f/x_i)$ is the variance of $E(f/x_i)$, and $V(f)$ is the overall variance of f. Generally, a large value of $S(x_i)$ reveals a strong influence on the optimization objective. Thus, the sensitivity of each design variable on the three optimization objectives can be calculated based on (2).

TABLE III
CONTROL FACTORS AND RANGES

Control factor	Unit	Ranges
θ_{on}	deg.	[-4, -2]
θ_{off}	deg.	[10, 12]
n	-	[20, 26]
D_{ro}	mm	[75, 85]
β_{s1}	deg.	[18, 21.5]
β_r	deg.	[24, 30]
g	mm	[0.25, 0.5]

Fig. 7 shows sensitivity analysis results for the SRM drive system. The angle position control (APC) method is utilized in this example. In terms of the comprehensive influence on the three optimization objectives, seven significant parameters, i.e., θ_{on}, θ_{off}, g, n, β_r, β_{s1}, and D_{ro} are selected as the control factors. Tables III lists the ranges for control factors. To find the noise factors of this structure, a criterion is proposed to determine the influence of uncertainties:

$$N(x_i) = S(x_i) \cdot \frac{\Delta x_i}{x_{i\_initial}} \tag{3}$$

where Δx_i is the manufacturing tolerance of x_i, and $x_{i\_initial}$ is the initial value of x_i.

Fig. 8 illustrates the influence of uncertainties based on the calculation of (3). As shown, the uncertainty of the air gap g has a high impact on the performance of this type of motor where the others only have little influence due to that the air gap g exhibits the highest value of $\Delta x_i/x_{i\_initial}$. Thus, g is determined as the noise factor with the two levels of -0.02 and +0.02 mm, where -0.02 mm means subtracting 0.02 mm from the initial value and +0.02 mm means adding 0.02 mm to the initial value.

TABLE IV
ORTHOGONAL ARRAY OF SLSTM

No	θ_{on}	θ_{off}	n	D_{ro}	β_{s1}	β_r	g
1	1	2	3	1	3	3	3
2	1	3	2	3	1	3	2
3	3	3	3	3	3	2	1
4	1	3	3	2	2	1	3
5	3	3	1	1	2	3	1
6	2	2	2	2	2	3	1
7	1	2	1	3	2	2	2
8	3	1	2	3	2	1	3
9	2	3	2	1	3	1	2
10	1	1	1	1	1	1	1
11	3	2	2	1	1	2	3
12	3	2	1	2	3	1	2
13	2	1	1	3	3	3	3
14	1	1	2	2	3	2	1
15	2	3	1	2	1	2	3
16	3	1	3	2	1	3	2
17	2	1	3	1	2	2	2
18	2	2	3	3	1	1	1

Step 3: Generate the orthogonal array and implement the simulations.

An orthogonal array generated from the control factors is listed in Table IV. The numbers in Table IV are corresponding

to the levels of control factors listed in Table V. During one iteration, 36 (18x2) combinations of FEM simulations will be performed where 18 is the row number of the orthogonal array for the control factors and 2 is the combination of the noise factor corresponding to the levels of -0.02 and +0.02 mm. Taking the first row in Table IV as an example, the values of θ_{on}, θ_{off}, n, D_{ro}, β_{s1}, and β_r corresponding to their levels are -4º, 11º, 26, 75 mm, 21.5º, and 30º, respectively, and g has two values, i.e., 0.48 mm (0.5-0.02) and 0.52 mm (0.5+0.02).

TABLE V
LEVELS FOR CONTROL FACTORS OF SLSTM IN EACH ITERATION

Control factor	Level	Iteration 1	Iteration 2	Iteration 3
θ_{on} (deg.)	1	-4	-3.5	-3.3
	2	**-3**	**-3**	**-3**
	3	-2	-2.5	--2.8
θ_{off} (deg.)	1	**10**	**10**	**10**
	2	11	10.5	10.3
	3	12	11	10.5
n	1	20	**21**	**21**
	2	**23**	23	22
	3	26	25	23
D_{ro} (mm)	1	75	80	82.5
	2	80	82.5	83.8
	3	**85**	**85**	**85**
β_{s1} (deg.)	1	18	19.8	20.6
	2	19.8	20.6	21.1
	3	**21.5**	**21.5**	**21.5**
β_r (deg.)	1	24	**27**	**27**
	2	27	28.5	27.8
	3	**30**	30	28.5
g (mm)	1	**0.25**	0.25	**0.31**
	2	0.38	0.31	0.35
	3	0.5	**0.38**	0.38

Step 4: Compute the S/N ratio and select the best value of each control factor.

According to the data obtained from the FEM samples, the signal/noise (S/N) ratio can be computed to find the optimal combination of control factors' levels. Two main steps should be accomplished to compute the S/N ratios. First, the S/N ratio for each row of the orthogonal array is calculated by

$$SN(i) = -10 \times \lg[\frac{1}{2} \times \sum_{j=1}^{2} F^2(i, j)] \quad (4)$$

where lg means the logarithm operator, and i and j are the row number in Table IV and the index of the noise factor, respectively.

Then, the average S/N ratios for all levels of optimization variables based on the S/N ratios of each row are computed. For example, the average S/N ratio for the first level of θ_{on} is the average value of $SN(1)$, $SN(2)$, $SN(4)$, SN(7), $SN(10)$ and $SN(14)$. The combination of the best design levels for the optimization variables can be determined by the S/N ratios. The higher S/N ratio means higher robustness. Thus, the level of each optimization variable which reveals the highest S/N ratio is selected.

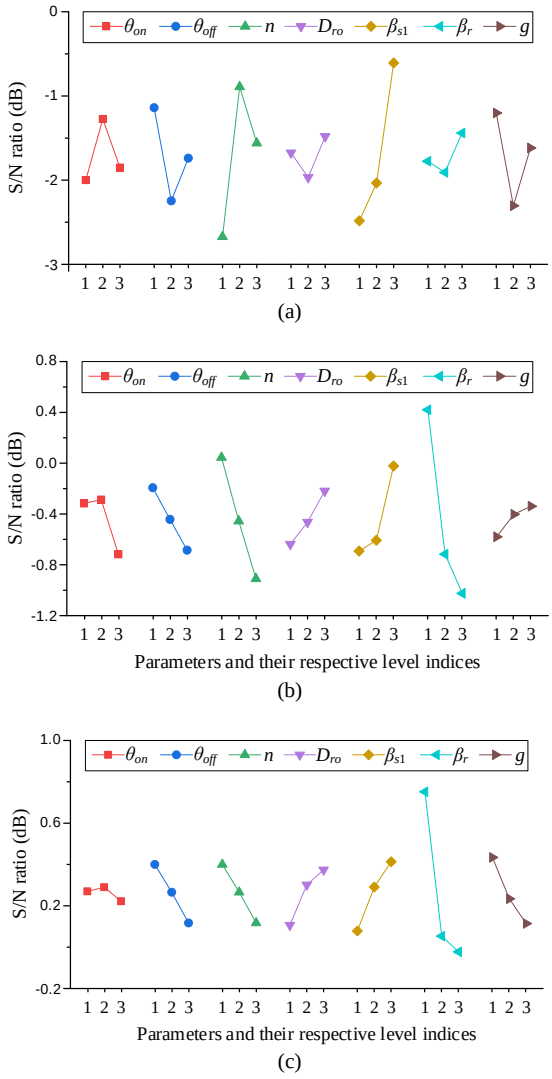

Fig. 9. S/N ratios of Iteration 1, (b) Iteration 2, and (c) Iteration 3 by using SLSTM.

Step 5: Calculate the value of the optimization function.

The value of the optimization function for the combined values of each parameter at the present iteration is calculated in this step. Steps 2~5 are considered as one iteration process, which is the distinguished difference between the proposed SLSTM and the conventional Taguchi method.

Step 6: Termination judgement.

A convergence criterion has been set for the iterative process. After calculating the objective's value for the present selected combinations, it is compared with the previous value. If the relative error is larger than 0 but less than ε, terminate the iterative process and output the optimal design. Otherwise, go to the next step and perform the next iterative process. In this example, ε is set to 1%.

The space reduction method is defined as follows for the transition to the next iteration step. Define [a, b] as the initial space of one control factor and L as the step size of the three levels. Besides, the step size of each control factor will be halved in the next iterative process. Assume the best value of the control factor is x_0, then the design levels of the next

iterative process will be calculated by

$$\begin{cases} (a, a+L/2, a+L), & x_0 - L/2 < a \\ (b-L, b-L/2, b), & x_0 + L/2 > b \\ (x_0 - L/2, x_0, x_0 + L/2), & others \end{cases}. \quad (5)$$

The S/N ratios by using the SLSTM of each iteration are illustrated in Fig. 9. As shown in Fig. 9(a), the best levels in Iteration 1 for the seven control factors (θ_{on}, θ_{off}, n, D_{ro}, β_{s1}, β_r and g) are 2, 1, 2, 3, 3, 3, and 1, which are corresponding to -3º, 10º, 23 mm, 85 mm, 21.5º, 30º and 0.25 mm, respectively. Taking θ_{on} as an example to explain (5) in more detail, the best value in Iteration 1 is -3º, as illustrated above. As the initial step is 1º, the next step is 0.5º. Since -3.5º (-3-0.5) is more than -4º and -2.5º (-3+0.5) is less than -2º, the next three levels of this control factor will be -3.5º, -3º, and -2.5º, respectively.

The best values of each parameter are presented in bold in Table V. The values of the optimization function F of the three iterations are 1.0502, 0.8670, and 0.8620, respectively. The relative error between Iterations 2 and 3 is 0.58%, which is less than ε. Thus, the iterative process will be terminated after the third iteration.

TABLE VI
ORTHOGONAL ARRAY OF CLSTM

No	n	D_{ro}	β_{s1}	β_r	g
1	2	2	2	2	1
2	2	4	3	1	3
3	1	2	3	4	2
4	3	3	3	3	1
5	1	1	1	1	1
6	1	4	2	3	4
7	3	1	2	4	3
8	1	3	4	2	3
9	4	3	2	1	2
10	2	3	1	4	4
11	3	4	1	2	2
12	2	1	4	3	2
13	4	1	3	2	4
14	3	2	4	1	4
15	4	4	4	4	1
16	4	2	1	3	3

IV. RESULTS AND COMPARISON

To better show the effectiveness of the proposed SLSTM, the component-level sequential Taguchi method (CLSTM) is performed for comparison. The only difference between the SLSTM and CLSTM is that the control factors selected from the control level are not included in CLSTM. Thus, in this example, θ_{on} and θ_{off} are excluded in CLSTM. The orthogonal array of CLSTM is presented in Table VI. It should be noted that each control factor has four levels, which is different from that of SLSTM due to the total number of control factors have been changed and a better orthogonal array is selected. Since it is a sequential Taguchi method presented in this paper, the final selection will gradually approach the optimal solution with the increase in the times of iterations. Thus, the number of levels has little influence on the final results and the fair comparison with SLSTM. Besides, a new space reduction formula is established as

$$\begin{cases} (a, a+L/2, a+L, a+3L/2), & x_0 - 3L/4 < a \\ (b-3L/2, b-L, b-L/2, b), & x_0 + 3L/4 > b \\ (x_0 - 3L/4, x_0 - L/4, & \\ x_0 + L/4, x_0 + 3L/4), & others \end{cases}. \quad (6)$$

The optimization flowchart of CLSTM is the same as that of the SLSTM. The levels for control factors of CLSTM are tabulated in Table VII. During one iteration, 32 (16x2) combinations of FEMs will be carried out where 16 is the row number of the orthogonal array for the control factors and 2 is the combination with the noise factor corresponding to the levels of -0.02 and +0.02 mm. The S/N ratios are illustrated in Fig. 10, corresponding selected results of each control factor for each iteration are presented in bold in Table VII. The values of the optimization function F of the three iterations are 1.1915, 1.0325, and 1.0228, respectively. The relative error between Iterations 2 and 3 is 0.94%, which is less than ε. Thus, the iterative process will be terminated after the third iteration.

The comparison of torque curves among the initial, CLSTM, and SLSTM designs is presented in Fig. 11. Detailed comparisons are presented in Table VIII. Moreover, to further compare the robustness performance of the three designs, a set of input data about the air gap which conforms to the normal distribution after verification are randomly generated. The distribution of data in each interval is presented in Fig. 12. The FEMs according to the different values of the air gap are established. After the simulation, the corresponding output results of F are presented in Fig. 13.

TABLE VII
LEVELS FOR CONTROL FACTORS OF CLSTM IN EACH ITERATION

Control factor	Level	Iteration 1	Iteration 2	Iteration 3
n	1	20	**22**	**22**
	2	22	23	23
	3	**24**	25	23
	4	26	26	24
D_{ro} (mm)	1	75	75.8	78.3
	2	**78.3**	77.5	79.1
	3	81.7	79.1	80
	4	85	**80.8**	**80.8**
β_{s1} (deg.)	1	18	19.8	20.6
	2	19.2	20.3	20.9
	3	20.3	20.9	21.2
	4	**21.5**	**21.5**	**21.5**
β_r (deg.)	1	24	**27**	27
	2	26	28	**27.5**
	3	28	29	28
	4	**30**	30	28.5
g (mm)	1	0.25	0.27	0.33
	2	**0.33**	0.31	**0.35**
	3	0.42	0.35	0.37
	4	0.5	**0.39**	0.39

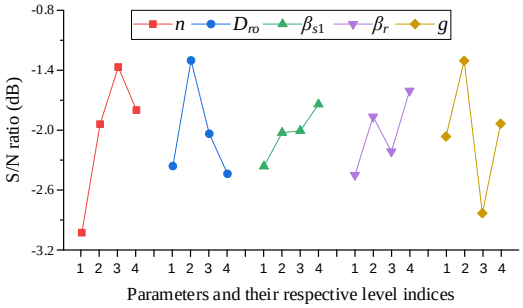

(a)

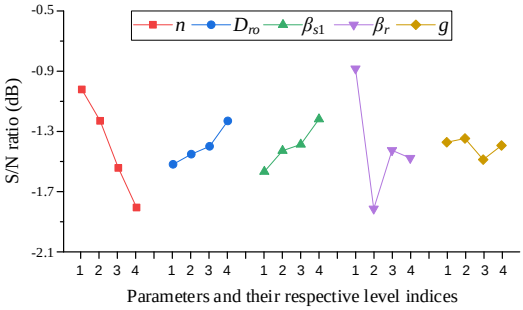

(b)

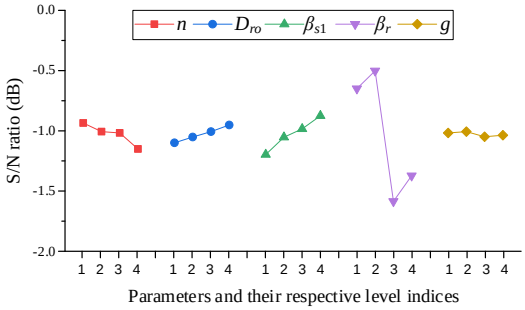

(c)

Fig. 10. S/N ratios of Iteration 1, (b) Iteration 2, and (c) Iteration 3 by using CLSTM.

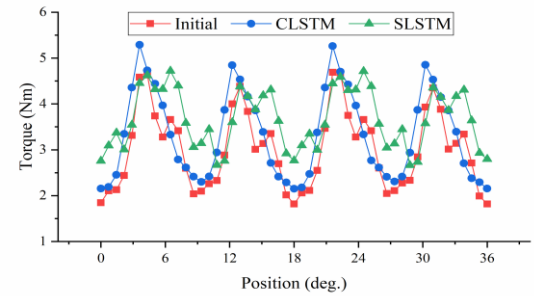

Fig. 11. Torque comparison for different designs.

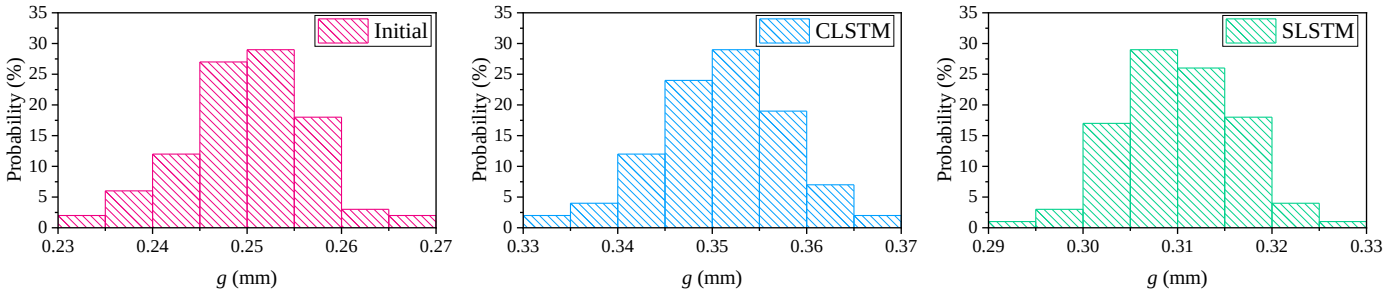

Fig. 12. Input data distribution of air gap for different designs.

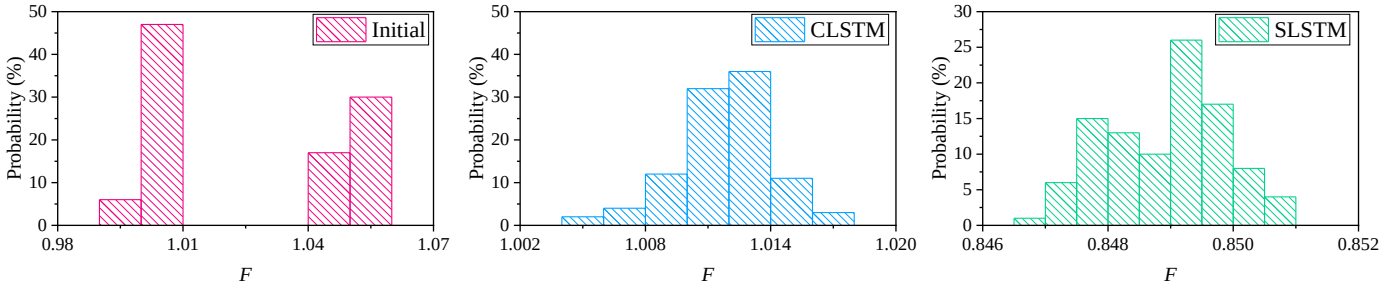

Fig. 13. Output results of F for different designs.

TABLE VIII
COMPARISON BETWEEN INITIAL, CLSTM, AND SLSTM DESIGNS

Par.	Unit	Initial	CLSTM	SLSTM
θ_{on}	deg.	-3	-3	-3
θ_{off}	deg.	12	12	10
n	-	24	22	21
D_{ro}	mm	82.00	80.8	85
β_{s1}	deg.	21.38	21.5	21.5
β_r	deg.	26.64	27.5	27
g	mm	0.25	0.35	0.31
T_{avg}	Nm	3.03	3.30	3.66
P_{loss}	W	195.06	225.45	218.17
T_{ripple}	%	93.64	96.28	61.08
F	-	1.00	1.0228	0.8620

The following conclusions can be drawn according to Figs. 11-13 and Table VIII.

1) For the CLSTM, the average torque, loss, torque ripple and the value of optimization function are 3.30 Nm, 225.45 W, 96.28%, and 1.0228, respectively. Compared with the initial

design, the average torque has been increased by about 8.91% while the loss is increased by 15.58%, and the torque ripple has been increased slightly. The overall output performance (represented by the value of optimization function *F*) is reduced by about 2.28%. It can be explained that, since the sequential Taguchi method aims to find a robust solution by the selection of levels with high S/N ratios, some performances will be sacrificed to some extent. Thus, it is reasonable that the value of *F* is higher than that of the initial design.

2) For the SLSTM, the average torque, loss, torque ripple and the value of optimization function are 3.66 Nm, 218.17 W, 61.08%, and 0.8620, respectively. Compared with the initial design, the average torque has been increased by about 20.79% with the sacrifice of 11.80% loss, the torque ripple has been greatly reduced by about 34.77%. Therefore, the overall performance has been improved by about 13.8%. Besides, the SLSTM exhibits higher average torque, less loss and lower torque ripple compared with CLSTM. It means the SLSTM exhibits the best overall output performance among the three designs.

3) Considering the robustness performance, from Fig. 13, it can be concluded that the initial design exhibits the lowest robustness, since *F* is distributed at both ends of the maximum and minimum values and achieves a range of 0.08 in *F* is observed, while those of CLSTM and SLSTM are only 0.013 and 0.005, respectively. The distributions of *F* in CLSTM and SLSTM are more concentrated and conform to the orthogonal distribution, which can verify the effectiveness of the sequential Taguchi method. Moreover, compared with the CLSTM, the distribution of *F* in SLSTM is narrower. This implies that the proposed SLSTM can achieve a higher level of robustness for SRM drive systems.

V. Conclusion

This paper presented a robust design optimization method of SRM drive systems with the consideration of manufacturing tolerances. A novel SLSTM was proposed to achieve the optimal solution with high robustness. The iterative process and the principle to sequentially reduce the considered design space have been presented. To show the effectiveness of the proposed method, a segmented-rotor SRM was investigated. Seven design parameters including two parameters related to control aspects and one noise factor were selected according to the sensitivity analysis. The CLSTM was performed for comparison. Compared with the initial design and the CLSTM, the proposed SLSTM can significantly improve motor performance like higher torque and lower torque ripple. Besides, it can provide a higher level of robustness.

References

[1] X. Sun, L. Feng, K. Diao, and Z. Yang, "An improved direct instantaneous torque control based on adaptive terminal sliding mode for a segmented-rotor SRM," *IEEE Trans. Ind. Electron.*, 2021 DOI: 10.1109/TIE.2020.3029463, to be published.

[2] X. Sun, Z. Shi, Y. Cai, G. Lei, Y. Guo, and J. Zhu, "Driving-cycle oriented design optimization of a permanent magnet hub motor drive system for a four-wheel-drive electric vehicle," *IEEE Trans. Transport. Electrific.*, vol. 6, no. 3, pp. 1115-1125, Sep. 2020.

[3] L. Sun, X. Li and L. Chen, "Motor Speed Control with Convex Optimization-based Position Estimation in the Current Loop," *IEEE Trans. Power Electron.*, 2021, DOI: 10.1109/TPEL.2021.3068309, to be published.

[4] X. Sun, K. Diao, G. Lei, Y. Guo, and J. Zhu, "Direct torque control based on a fast modeling method for a segmented-rotor switched reluctance motor in HEV application," *IEEE J. Emerg. Sel. Topics Power Electron.*, vol. 9, no. 1, pp. 232-241, Feb. 2021.

[5] D. Gerada, X. Huang, C. Zhang, H. Zhang, X. Zhang, and C. Gerada, "Electrical machines for automotive electrically assisted turbocharging," *IEEE/ASME Trans. Mechatron.*, vol. 23, no. 5, pp. 2054-2065, 2018.

[6] X. Sun, Y. Shen, S. Wang, G. Lei, Z. Yang, and S. Han, "Core losses analysis of a novel 16/10 segmented rotor switched reluctance BSG motor for HEVs using nonlinear lumped parameter equivalent circuit model," *IEEE/ASME Trans. Mechatronics*, vol. 23, no. 2, pp. 747-757, Apr. 2018.

[7] K. Diao, X. Sun, G. Lei, Y. Guo, and J. Zhu, "Multimode optimization of switched reluctance machines in hybrid electric vehicles," *IEEE Trans. Energy Convers.*, 2021, DOI: 10.1109/TEC.2020.3046721, to be published.

[8] X. Sun, K. Diao, G. Lei, Y. Guo, and J. Zhu, "Real-time HIL emulation for a segmented-rotor switched reluctance motor using a new magnetic equivalent circuit," *IEEE Trans. Power Electron.*, vol. 35, no. 4, pp. 3841-3849, Apr. 2020.

[9] W. Wang, M. Luo, E. Cosoroaba, B. Fahimi, and M. Kiani, "Rotor shape investigation and optimization of double stator switched reluctance machine," *IEEE Trans. Magn.*, vol. 51, no. 3, pp. 1-4, 2015.

[10] Y. K. Choi, H. S. Yoon, and C. S. Koh, "Pole-shape optimization of a switched-reluctance motor for torque ripple reduction," *IEEE Trans. Magn.*, vol. 43, no. 4, pp. 1797-1800, 2007.

[11] T. Raminosoa, B. Blunier, D. Fodorean, and A. Miraoui, "Design and optimization of a switched reluctance motor driving a compressor for a PEM fuel-cell system for automotive applications," *IEEE Trans. Ind. Electron.*, vol. 57, no. 9, pp. 2988-2997, 2010.

[12] I. Kioskeridis and C. Mademlis, "Maximum efficiency in single-pulse controlled switched reluctance motor drives," *IEEE Trans. Energy Convers.*, vol. 20, no. 4, pp. 809-817, 2005.

[13] S. F. Toloue, S. H. Kamali, and M. Moallem, "Torque ripple minimization and control of a permanent magnet synchronous motor using multiobjective extremum seeking," *IEEE/ASME Trans. Mechatron.*, vol. 24, no. 5, pp. 2151-2160, 2019.

[14] X. Sun, Z. Shi, G. Lei, Y. Guo, and J. Zhu, "Multi-objective design optimization of an IPMSM based on multilevel strategy," *IEEE Trans. Ind. Electron.*, vol. 68, no. 1, pp. 139-148, 2021.

[15] G. Bramerdorfer, J. A. Tapia, J. J. Pyrhönen, and A. Cavagnino, "Modern electrical machine design optimization: techniques, trends, and best practices," *IEEE Trans. Ind. Electron.*, vol. 65, no. 10, pp. 7672-7684, 2018.

[16] K. Diao, X. Sun, G. Lei, G. Bramerdorfer, Y. Guo, and J. Zhu, "System-level robust design optimization of a switched reluctance motor drive system considering multiple driving cycles," *IEEE Trans. Energy Convers.*, vol. 36, no. 1, pp. 348-357, 2021.

[17] B. Mirzaeian, M. Moallem, V. Tahani, and C. Lucas, "Multiobjective optimization method based on a genetic algorithm for switched reluctance motor design," *IEEE Trans. Magn.*, vol. 38, no. 3, pp. 1524-1527, 2002.

[18] J. Zhang, H. Wang, L. Chen, C. Tan, and Y. Wang, "Multi-objective optimal design of bearingless switched reluctance motor based on multi-objective genetic particle swarm optimizer," *IEEE Trans. Magn.*, vol. 54, no. 1, pp. 1-13, 2018.

[19] H. A. Moghaddam, A. Vahedi, and S. H. Ebrahimi, "Design optimization of transversely laminated synchronous reluctance machine for flywheel energy storage system using response surface methodology," *IEEE Trans. Ind. Electron.*, vol. 64, no. 12, pp. 9748-9757, 2017.

[20] S. I. Nabeta, I. E. Chabu, L. Lebensztajn, D. A. P. Correa, W. M. d. Silva, and K. Hameyer, "Mitigation of the torque ripple of a switched reluctance motor through a multiobjective optimization," *IEEE Trans. Magn.*, vol. 44, no. 6, pp. 1018-1021, 2008.

[21] K. Diao, X. Sun, G. Lei, Y. Guo, and J. Zhu, "Multiobjective system level optimization method for switched reluctance motor drive systems using finite-element model," *IEEE Trans. Ind. Electron.*, vol. 67, no. 12, pp. 10055-10064, 2020.

[22] C. Ma and L. Qu, "Multiobjective optimization of switched reluctance motors based on design of experiments and particle swarm optimization," *IEEE Trans. Energy Convers.*, vol. 30, no. 3, pp. 1144-1153, 2015.

[23] X. Sun, B. Wan, G. Lei, X. Tian, Y. Guo, and J. Zhu, "Multiobjective and multiphysics design optimization of a switched reluctance motor for

electric vehicle applications," *IEEE Trans. Energy Convers.*, 2021, DOI 10.1109/TEC.2021.3078547, to be published.
[24] G. Lei, T. Wang, J. Zhu, Y. Guo, and S. Wang, "System-level design optimization method for electrical drive systems—robust approach," *IEEE Trans. Ind. Electron.*, vol. 62, no. 8, pp. 4702-4713, 2015.
[25] Z. Shi, X. Sun, Y. Cai, and Z. Yang, "Robust design optimization of a five-phase PM hub motor for fault-tolerant operation based on Taguchi method," *IEEE Trans. Energy Convers.*, vol. 35, no. 4, pp. 2036-2044. Dec. 2020.
[26] S. Lee, K. Kim, S. Cho, J. Jang, T. Lee, and J. Hong, "Optimal design of interior permanent magnet synchronous motor considering the manufacturing tolerances using Taguchi robust design," *IET Elect. Power Appl.*, vol. 8, no. 1, pp. 23-28, 2014.
[27] X. Sun, Z. Shi, and J. Zhu, "Multi-objective design optimization of an IPMSM for EVs based on fuzzy method and sequential Taguchi method," *IEEE Trans. Ind. Electron.*, 2021 DOI: 10.1109/TIE.2020.3031534, to be published.
[28] B. C. Mecrow, E. A. El-Kharashi, J. W. Finch, and A. G. Jack, "Preliminary performance evaluation of switched reluctance motors with segmental rotors," *IEEE Trans. Energy Convers.*, vol. 19, no. 4, pp. 679-686, 2004.
[29] J. D. Widmer, R. Martin, and B. C. Mecrow, "Optimization of an 80-kW segmental rotor switched reluctance machine for automotive traction," *IEEE Trans. Ind. Appl.*, vol. 51, no. 4, pp. 2990-2999, 2015.
[30] Z. Xu, D. Lee, and J. Ahn, "Design and operation characteristics of a novel switched reluctance motor with a segmental rotor," *IEEE Trans. Ind. Appl.*, vol. 52, no. 3, pp. 2564-2572, 2016.

Kaikai Diao (S'18) was born in Zhenjiang, Jiangsu, China, in 1994. He received the B.S. degree in vehicle engineering from Jiangsu University, Zhenjiang, China, in 2017, and he is currently working toward the Ph.D. degree in Jiangsu University, Zhenjiang, China.

His current research interests include design, optimization, magnetic equivalent circuits modeling, control, and loss analysis of switched reluctance motors for automobile application.

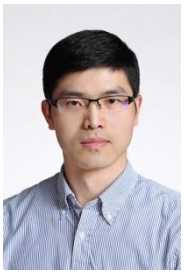

Xiaodong Sun (M'12-SM'18) received the B.Sc. degree in electrical engineering, and the M.Sc. and Ph.D. degrees in control engineering from Jiangsu University, Zhenjiang, China, in 2004, 2008, and 2011, respectively.

Since 2004, he has been with Jiangsu University, where he is currently a Professor in Vehicle Engineering with the Automotive Engineering Research Institute. From 2014 to 2015, he was a Visiting Professor with the School of Electrical, Mechanical, and Mechatronic Systems, University of Technology Sydney, Sydney, Australia. His current teaching and research interests include electrified vehicles, electrical machines, electrical drives, and energy management. He is the author or coauthor of more than 100 refereed technical papers and one book, and he is the holder of 42 patents in his areas of interest. Dr. Sun is an Editor of the IEEE TRANSACTIONS ON ENERGY CONVERSION.

Gang Lei (M'14) received the B.S. degree in Mathematics from Huanggang Normal University, China, in 2003, the M.S. degree in Mathematics and Ph.D. degree in Electrical Engineering from Huazhong University of Science and Technology, China, in 2006 and 2009, respectively.

He is currently a Senior Lecturer at the School of Electrical and Data Engineering, University of Technology Sydney (UTS), Australia. His research interests include computational electromagnetics, design optimization and control of electrical drive systems and renewable energy systems. He is an Associate Editor of the IEEE TRANSACTIONS ON INDUSTRIAL ELECTRONICS and an Editor of the IEEE TRANSACTIONS ON ENERGY CONVERSION.

Gerd Bramerdorfer (S'10-M'14-SM'18) received the Ph.D. degree in electrical engineering from Johannes Kepler University Linz, Linz, Austria, in 2014. He is currently an Assistant Professor with the Department of Electrical Drives and Power Electronics, Johannes Kepler University Linz. His research interests include the design, modeling, and optimization of electric machines as well as magnetic bearings and bearingless machines.

Dr. Bramerdorfer is a Senior Member of IEEE, an Editor of the IEEE TRANSACTIONS ON ENERGY CONVERSION and a past Associate Editor of the IEEE TRANSACTIONS ON INDUSTRIAL ELECTRONICS.

Youguang Guo (S'02-M'05-SM'06) received the B.E. degree from Huazhong University of Science and Technology, China in 1985, the M.E. degree from Zhejiang University, China in 1988, and the Ph.D. degree from University of Technology, Sydney (UTS), Australia in 2004, all in electrical engineering.

He is currently a Professor at the School of Electrical and Data Engineering, University of Technology Sydney (UTS). His research fields include measurement and modeling of properties of magnetic materials, numerical analysis of electromagnetic field, electrical machine design optimization, power electronic drives and control.

Jianguo Zhu (S'93–M'96–SM'03) received the B.E. degree in 1982 from Jiangsu Institute of Technology, Jiangsu, China, the M.E. degree in 1987 from Shanghai University of Technology, Shanghai, China, and the Ph.D. degree in 1995 from the University of Technology Sydney (UTS), Sydney, Australia, all in electrical engineering.

He was appointed a lecturer at UTS in 1994 and promoted to full professor in 2004 and Distinguished Professor of Electrical Engineering in 2017. At UTS, he has held various leadership positions, including the Head of School for School of Electrical, Mechanical and Mechatronic Systems and Director for Centre of Electrical Machines and Power Electronics. In 2018, he joined the University of Sydney, Australia, as a full professor and Head of School for School of Electrical and Information Engineering. His research interests include computational electromagnetics, measurement and modelling of magnetic properties of materials, electrical machines and drives, power electronics, renewable energy systems and smart micro grids.